COMSOL Multiphysics® Implementation of a Genetic Algorithm Routine for Metasurface Optimization

Bryan M. Adomanis*[1], D. Bruce Burckel[2], and Michael A. Marciniak[1]
[1]Department of Engineering Physics, Air Force Institute of Technology, 2950 Hobson Way, Wright-Patterson Air Force Base, OH 45433-7765
[2]Sandia National Laboratories, P.O. Box 5800, Albuquerque, New Mexico 87185
*Corresponding author: bryan.adomanis@us.af.mil

Abstract:

Keywords: metasurfaces, flat lens, optimization

1. Introduction

In recent years, metasurfaces have been shown to control the phase and amplitude of light across a planar interface, primarily implemented for demonstration optical functions of beam-steering, focusing, and polarization rotation [1]. Initial efforts using plasmonic-based scatterers proved successful in achieving the desired functionality; however, these plasmonic designs exhibited limitations in efficiency that stifled further academic vigor, as researchers shifted interest to higher-efficiency dielectric-based designs [2, 3].

The source of these limitations stem from fundamental behaviors of scattering at a subwavelength interface [4, 5], where field interactions occur over the thickness of the source inclusion (t), which is much smaller than the wavelength in the surrounding medium (λ_0/n). This small distance impedes significant accumulation of phase in transmission across the interface, and inevitably caps the theoretical maximum efficiencies these structures can generate.

Here, we continue the investigation of plasmonic structures for metasurface-based optics by implementing 3-D designs. This additional dimension allows for intricate electromagnetic interactions, to include coupling between in-plane (IP) and out-of-plane (OOP) scatterers, and the incident magnetic field component with the OOP scatterer. These interactions potentially offer access to a greater range of phase space.

This high level of subwavelength interaction makes analytical solutions challenging, if not impossible. To accurately assess if these structures could provide efficient phase control for beam-shaping, we utilized COMSOL Multiphysics® for determination of the scattered field. To preclude the need to discretely sample all points of the amplitude/phase trade space, we implemented COMSOL's LiveLink™ for MATLAB® to derive a genetic algorithm (GA) optimization routine that would hone in on the desired result.

In this paper, we first show how the GA routine can utilize a multi-objective fitness function to select a free-space Huygens-like scatterer—one which maximizes forward scatter and minimizes backscatter. We then move to a unit cell analysis of a more realistic structure consisting of an array of gold (Au) voxels embedded in a silicon (Si) substrate cavity over periodic boundary conditions, demonstrating that the COMSOL-based GA routine can generate a 3-D unit cell that effectively hits a given phase target at maximum amplitude. Finally, alternate basis voxels are explored for mitigation of fabrication challenges.

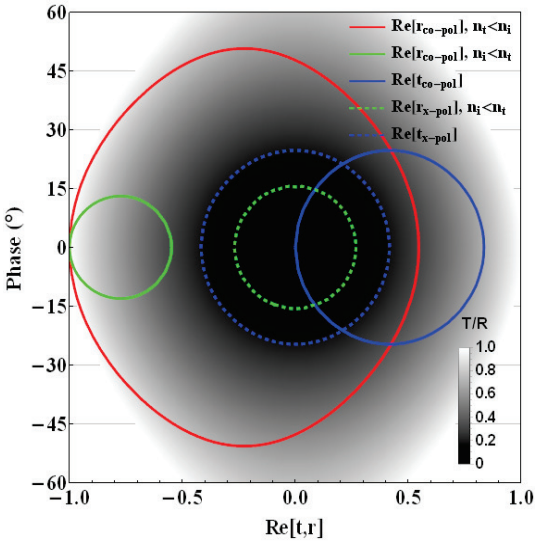

Figure 1. Complex plot of Im[t,r] (in terms of phase) vs Re[t,r] for 2-D planar structures with uniform, discretized surface currents for co-polarized (solid) and cross-polarized (dashed) transmission (blue) and reflection (green, red). Density profile gives transmittance/reflectance intensities.

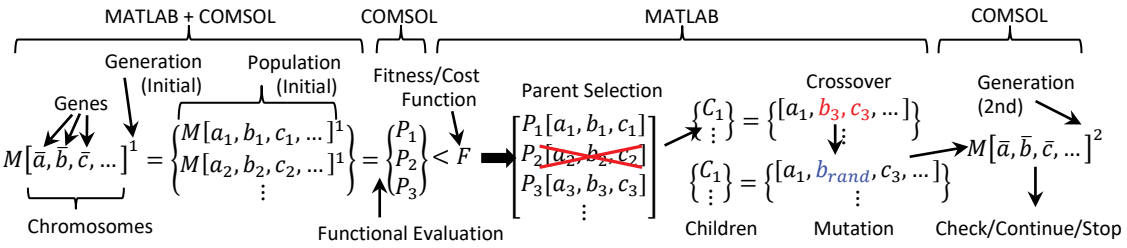

Figure 2. Overview of the genetic algorithm routine, showing COMSOL/MATLAB roles.

2. Motivation

2.1 Limitations of Planar Metasurfaces

Many papers in the past five years have laid the theoretical groundwork on metasurfaces and demonstrated a variety of optical functions through both plasmonic and dielectric designs. The reader is directed to several papers for proper orientation $[\mathbf{1}, \mathbf{6-9}]$. Here, we cover some of the limitations from previous metasurface works.

For light illuminating a surface with only constant, discretized electric current densities (i.e. no magnetic or intra-cell coupling), it can be shown using Fresnel transmission and reflection coefficients $\{\boldsymbol{t}, \boldsymbol{r}\}$ that the phase range of light is bounded at $(\mathbf{-90°}, \mathbf{90°})$ for two lossless media of arbitrary refractive indices [4, 5]. Using the seminal Au/Si V-antenna planar structures ($\boldsymbol{n} = \mathbf{3.42\ at\ 8}\boldsymbol{\mu m}$), the limits on the amplitude and phase of $\boldsymbol{t}$ (blue) and $\boldsymbol{r}$ (red, green) are shown in Fig.1 for co-polarized (line) and cross-polarized (dashed) light. The background density (greyscale) shows the resultant transmission and reflection intensities $\{\boldsymbol{T}, \boldsymbol{R}\} = |\{\boldsymbol{t}, \boldsymbol{r}\}|^{\mathbf{2}}$, and $\{\boldsymbol{n_i}, \boldsymbol{n_t}\}$ are the refractive indices for the incident and transmitting media, respectively. This figure indicates that for co-polarized light there is high potential $\boldsymbol{T}$, though this suffers when spanning the phase space; conversely, the cross-polarized light spans phase at a constant, but low $\boldsymbol{T}$.

Ultimately, Fig.1 indicates that a planar metasurface cannot overcome its opposing physical limitations. One solution to this dilemma may exist in 3-D structures. First, a larger phase space should be available by coupling the incident light into both electric and magnetic fundamental modes, both in-plane and out-of-plane, rather than just electric, in-plane modes for 2-D structures. Second, since a 2-D subwavelength antenna behaves similar to a Hertzian dipole [6], this means the radiation pattern is limited due to the equal distribution of forward and backward scatter. There is no such explicit limitation in 3-D scatterers, however, and a preferential forward scatter is possible by careful superposition of electric and magnetic sources—such structures are often called "Huygens sources." Thus, the combination of a wide span of phase with strong preferential forward scattering amplitude should provide a much improved transmit-array for optical applications.

However, the major drawback of 3-D structures is in the increased complexity in design. This leaves it challenging to analytically determine scattered phase and amplitude in such 3-D subwavelength periodic structures, where strong inter-cell and intra-cell coupling can occur in the near-field regime. Furthermore, there is a strong uncertainty in what design is optimal for a desired phase value. Therefore, COMSOL was combined with a genetic algorithm through LiveLink for MATLAB to identify the optimal scatterer design.

2.2 Overview of Genetic Algorithms

A genetic algorithm is a specific type of evolutionary algorithm, which does exactly as it sounds: evolves primal solutions into refined solutions. It does so by selecting the most "fit" designs and altering their parameters to form new, potentially more optimal designs. Refer to Fig.2 and recommended textbooks [7, 8] in the following description of the GA process.

The GA begins by identifying a "chromosome," which consists of the set of "genes" (parameters) that define a unique "individual" (design), such as geometry, periodicity, incidence angle—any of the parameters commonly used in a COMSOL sweep. These genes can be coded as real-valued, such as some dipole length $\boldsymbol{L} = \mathbf{0.955}\boldsymbol{\mu m}$, or binary, where a real value is coded into a binary string of an appropriate size, such as $\boldsymbol{L} = \mathbf{0.955}\boldsymbol{\mu m} \Leftrightarrow \mathbf{11001}$ for a 5-bit string.

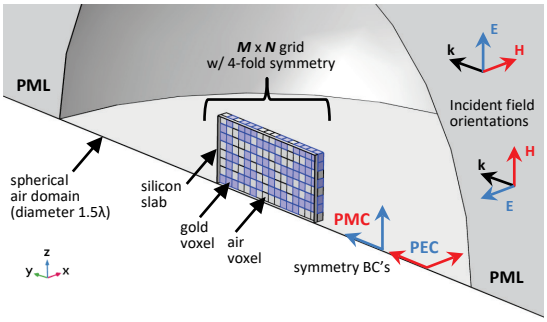

Figure 4. COMSOL model for 2-layer grid.

Each individual is associated with a single solution, so a large number of individuals (a multiplicative factor times # genes) are run to serve as a sufficiently diverse "population" of solutions to down-select against a fitness function, with the best fit individuals given the largest weighted, normalized score.

The "parents" used to create the "children" of the next "generation" of populations are chosen in two steps. The highest scoring $\mathbf{25\% - 50\%}$ of the initial generation is set aside as new children. This is called a "steady-state" approach, which ensures the many of the fittest individuals exist in the next generation. Next, the entire population participates in a tournament-style selection process, grabbing 3-5 individuals and picking one with the highest score—this becomes one parent.

Another parent is selected in the same manner, and these two designs undergo the fundamental evolutionary operator, called a "crossover," which exchange genes at some random point in the gene string. In Fig.2, this shows that parent #1 $(\boldsymbol{P_1})$, with genes $(\boldsymbol{a_1}, \boldsymbol{b_1}, \boldsymbol{c_1}, \dots)$ switches genes with another parent with genes $(\boldsymbol{a_3}, \boldsymbol{b_3}, \boldsymbol{c_3}, \dots)$ at index #2 (gene $\boldsymbol{b}$), such that child #1 $(\boldsymbol{C_1})$ has a chromosome of $(\boldsymbol{a_1}, \boldsymbol{b_3}, \boldsymbol{c_3}, \dots)$. A new set of parents are selected for the next child, and this process repeats until the remaining $\mathbf{50\% - 75\%}$ children fill out the rest of the population. This is the new generation, to be solved, fitted and to serve as the next set of parents.

GA methods are global optimizers, which means one should expect the solution to not be a local extrema, but the largest extrema in the set of all solutions, to within tolerances. The mechanism which allows this is called a "mutation." Mutations can help eject solutions that are stuck in a local extrema to a new location in solution space, to converge towards a new extrema. After a population of children are selected, a small percentage of genes are randomly mutated ($< \mathbf{5\%}$), having the value of that gene is altered; for a binary-coded gene, this

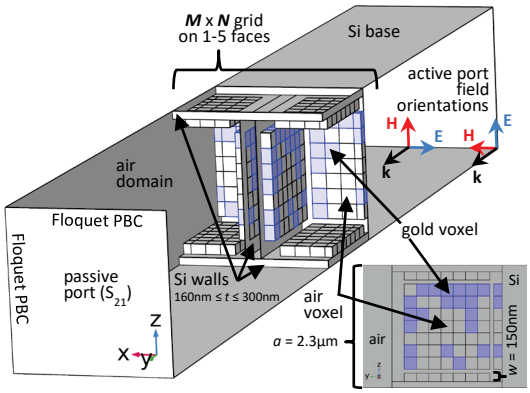

Figure 3. COMSOL model for MPL structure.

is as simple as flipping a single bit in the string from 1 to 0. In Fig.2, this is shown by changing gene $\boldsymbol{b_3}$ (red) in $\boldsymbol{C_1}$ to the value $\boldsymbol{b_{rand}}$ (blue).

3. COMSOL Multiphysics® Model

This work utilizes a bi-directional process link between COMSOL and MATLAB via LiveLink to identify models which exhibit a maximum uniform amplitude at an assortment of field phase values required to construct a flat metasurface lens. The governing program was created using COMSOL's application programming interface (API), and is fully-automatic: once a user selects certain parameters—such as desired phase value, tolerance, and number of populations—the process generates populations (models) with random genes, obtains solutions of the scattered and/or total electric fields, calculates desired values (e.g. phase and amplitude), performs the GA optimization routine, creates the next generation of COMSOL models, and iterates until a given stop criterion.

The central focus of the optimization is the scatterer, which, as shown in Fig.3, is manifest in the form of an $M \; x \; N$ grid of voxels identified as either a dielectric (air) or a metal (gold). Each gene is essentially the identifier of an individual voxel in the grid, with a "0" representing air and a "1" representing gold, such that the resulting model has an array of metal voxels which produce the optimal results. This makes the chromosome the set of $N \; x \; M$ binary representations, arrayed in a sequential order according to how COMSOL numbers the domains. For example, in a $10 \; x \; 10$ grid, the voxel closest to the origin is given the lowest domain index (say, "7", after COMSOL counts the enveloping spherical domain features) and represents gene #1. The GA program then assigns genes sequentially up to #100 (as domain

index “106”) and keeps track of this relation for future evolution operations (crossover, mutation).

3.1 The Validation Model

Two primary models were simulated. The first was a simplified model (Fig.3) used to validate the GA routine, consisting of one or two out-of-plane grids isolated in air, and sandwiching a silicon dielectric slab.

The fitness function was multi-objective, seeking an optimal Huygens source that exhibits maximum forward scatter and maximum difference between forward and backward scatter, as given by:

$$F\left(w_\Delta, w_f\right) = w_\Delta \frac{\Delta|\boldsymbol{E}|^2 - \min\left(\Delta|\boldsymbol{E}|^2\right)}{\max\left(\Delta|\boldsymbol{E}|^2\right) - \min\left(\Delta|\boldsymbol{E}|^2\right)} + w_f \frac{|\boldsymbol{E}^f|^2 - \min\left(|\boldsymbol{E}^f|^2\right)}{\max\left(|\boldsymbol{E}^f|^2\right) - \min\left(|\boldsymbol{E}^f|^2\right)} \quad [1]$$

where $\Delta|\boldsymbol{E}|^2 = \left|\boldsymbol{E}^f\right|^2 - \left|\boldsymbol{E}^d\right|^2$ is the difference between the forward and back scattered far fields, respectively, and w_Δ, w_f are the associated weights.

To starkly demonstrate the benefit of out-of-plane antennas, the field values were baselined against fields of an optimized in-plane V-antenna, such that "dBv" is the field value in decibels referenced to this V-antenna. Being on a dB scale, the min() function was required to account for negative values, and the dominators perform the normalization of the fields, so that $0 \leq F \leq 1$.

For calculation of the scattered fields, the Wave Optics module was used in conjunction with the Far-Field Domain feature using perfectly-matched layers to cut-off the computational domain. Domain Point Probes captured the far field values at singular points (forward at 0° to incidence vector along $+\hat{y}$ direction and backward at $-\hat{y}$). Perfect electrical conductors (PECs) and perfect magnetic conductors (PMCs) were used to avail 4-fold symmetry. This prevented any asymmetrical designs, but served its purpose for the GA validation.

3.2 The MPL Model

The second model as shown in Fig.4, and represents a more realistic structure. To produce an out-of-plane grid that could be fabricated, we based this model on Sandia National Laboratories’ membrane projection lithography (MPL) design phenomenology [9]. The MPL structure is a periodic unit cell of a silicon cube which has a cubic air cavity carved out. After applying a membrane mask, the four vertical faces and the single floor face can be decorated with any metallic pattern that does not require closed loops, as the membrane would have no support, otherwise. Note in Fig.4 the y/z wall was shifted to the center to reduce domain meshing while still allowing easy tracking of domain indices on at least two faces.

Our goal with this model was to produce a series of periodic unit cells which have maximum transmissivity at a series of selected phase points. Therefore, now the total field is of primary interest, as we wish to improve transmission efficiency of a metasurface lens without the need for polarization rotation into a cross-polarized field, which carry the limitations as noted previously. Hence, we eliminate PEC/PMC/PML boundary conditions and an incident background field in favor of periodic boundary conditions (PBCs) and active/passive ports. Similarly, the fitness function must also change, as we are targeting a particular value of phase, not an extrema. Thus, we needed a peak function with an allowable deviation for the phase term, where fitnesses outside a standard deviation (σ) rapidly drop off, such as a Lorentzian:

$$F\left(w_\Phi, w_f\right) = w_\Phi \frac{\sigma_\Phi^2}{|\Phi - \Phi_0|^2 + \sigma_\Phi^2} + w_s \frac{\sigma_s^2}{||S_{21}|^2 - \mathrm{T_0}| + \sigma_s^2} \quad [2]$$

where Φ, Φ_0 are the simulated and target phase points, respectively, $|S_{21}|^2$ is the transmission intensity at the passive port, and w_Φ, w_s are the weights for the transmission phase and intensity terms. It was found a good value for σ_Φ was around 10°, which gives enough room for viable phase points to be found in regions that are difficult to access.

While periodicity (a), wall thickness (t) and metal thickness (w) can be additional design parameters, a was fixed at $2.3\mu m$ (just below diffraction edge for $8\mu m$ light), w was fixed at $150nm$, and t was allowed to vary in some simulations between $160nm - 300nm$, to investigate the effect on inter-cell coupling.

No symmetry conditions were applied, because a primary interest was to mitigate restrictions on the grid; in addition, the cross-polarization would have been lost. Despite the lack of symmetry in the full model, each solution

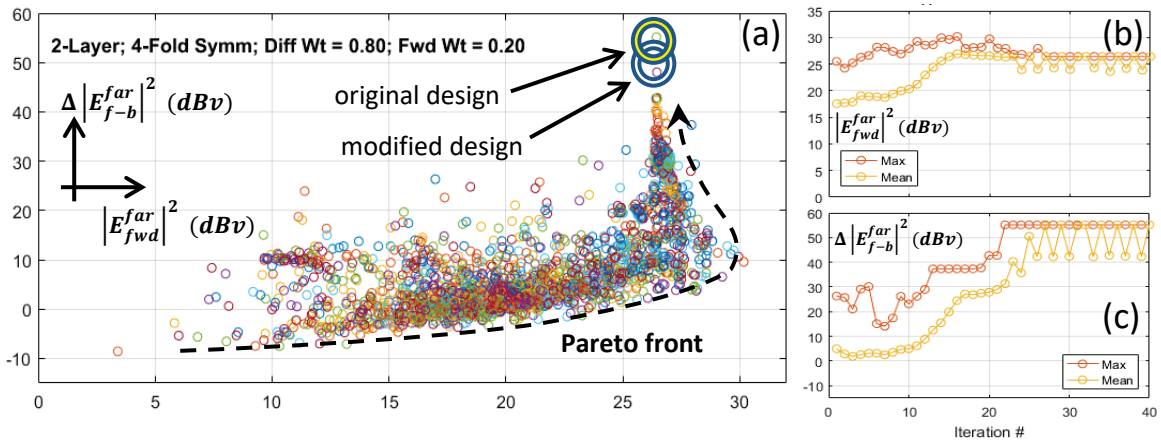

Figure 5. (a) Results of converged GA solution for a 2-layer, 4-fold symmetrical model, maximizing scattered forward far-field and the forward/backward difference, with "best" result highlighted (yellow). The convergence of the mean (orange) and max (red) of the forward (b) and difference (c) fields.

required ~5/7.5GB physical/virtual memory, with ~40K domain meshes and ~250K degrees of freedom. Using a 2 CPU/28-core/256GB workstation, each solution took approximately 30s, and computation times can be extrapolated from the desired population (N_{pop}) and iteration (N_{iter}) sizes. Generally, a factor of two was applied to the grid size, such that $Npop = 2xMxN$, and convergences occurred typically for $Niter < 20$.

4. COMSOL Simulation Results

While it is not possible to show the range of results that emerged from the myriad of design options (single-face, multi-face, symmetrical, asymmetrical, vertical/horizontal polarization), some representative results will be highlighted. In all examples, the incident field was oriented in the $\hat{z}$-direction and propagated in the $\hat{y}$-direction, which both align in the plane of the grids.

4.1 Validation of the GA Routine

A validation of the GA routine is presented in Fig.5 for a 2-layer symmetrical $16x16$ grid using an initial population of $N_{pop} = 120$. The solution space (a) is plotted in terms of the two maximums desired: $\Delta|\boldsymbol{E}|^2$ vs. $|\boldsymbol{E}^f|^2$, in dBv, and with a heavy weight towards the scattering difference, such that $\{w_\Delta, w_f\} = \{0.8, 0.2\}$. A Pareto front is clearly seen (dashed), defining the theoretical boundary limit of possible solutions. While the maximum forward scatter is around 30dBv, it comes with a significant 20dBv backscatter. Another solution along the front may be considered more optimal, with a forward scatter of 26dBv and practically negligible backscatter of -28dBv.

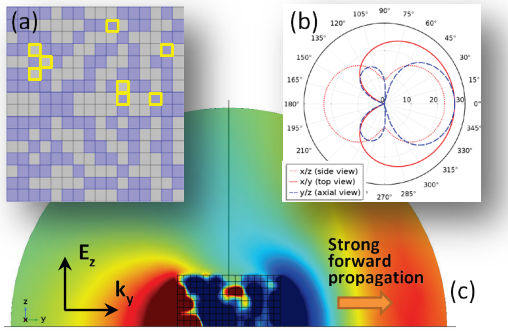

Figure 6. (a) Grid layout from "best" solution given in Fig.5(a). Far-field radiation pattern in 2-D (b) shows strong forward scatter, as well as in the near field (c).

However, Fig.5(a) does not alone demonstrate that the GA code is converging. Figs.5(b-c) show the evolution of the max (red) and top 50% mean (orange) of $|\boldsymbol{E}^f|^2$ and $\Delta|\boldsymbol{E}|^2$, respectively, over successive iterations. By the 22nd iteration, both global extremes were attained, though $|\boldsymbol{E}^f|^2$ receded to compensate for the higher weight toward $\Delta|\boldsymbol{E}|^2$. Oscillations in the mean occur after this due to the high sensitivity of very low intensities, introduced by slight changes to the design through the GA mutation operator.

For this example, the "best" design is considered the 26dBv/-28dBv solution, circled in yellow in Fig.5(a) and shown in detail in Fig.6. Fig.6(a) shows the layout of gold (blue) and air (grey), mirrored to show the full $16x16$ grid. Strong localized variations in the H_x field can be seen in the near-field (c), induced by circulation of current density in the voxel pattern. Forward propagation is quickly dominating well within the 0.75λ air domain radius. The far field radiation pattern in 2-D (b) shows that while some minor sidelobes exist in the y/z plane, and the x/y plane

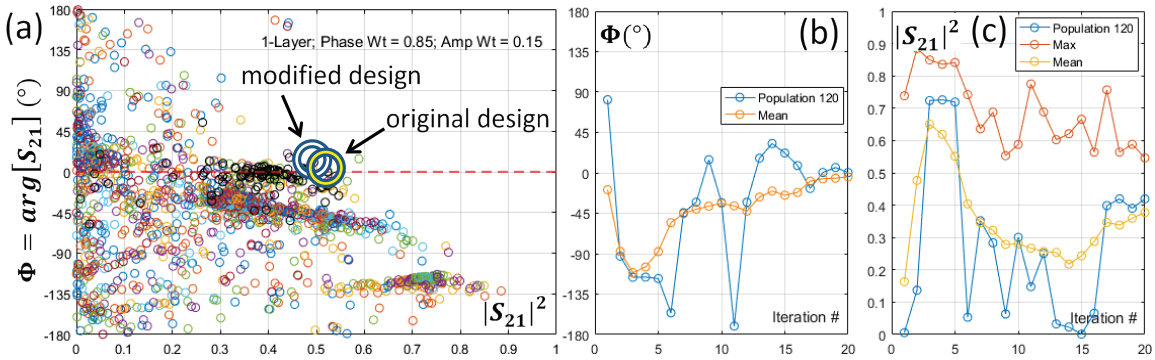

Figure 7. **(a)** Results of converged GA solution (black) for a 1-layer, asymmetrical MPL structure, targeting 0° phase (dashed). The convergence of the of $\boldsymbol{T}$ (b) and phase (c) in terms of mean (orange), max (red) and an individual population (blue).

has a wide spread, this profile is very close to a Huygens-like source.

Nevertheless, this design is not feasible for fabrication, as membrane masks cannot have a closed loop. Therefore, the voxels highlighted in yellow in Fig.6(a) had their material flipped (metal↔dielectric), such that all remaining loops were now open. The result (Fig.5(a), white) was only a 10dBv increase in backscatter, which is still ~25dB lower than the V-antenna.

4.2 Applying GA to MPL Structure

After a successful demonstration of the GA routine on a simple model gave high confidence to move toward the complex structure. The GA results for a $7x9$ 1-face asymmetrical MPL structure are shown in Fig.7(a), using $N_{pop} = 120$, $N_{iter} = 15$, and $\{w_\Phi, w_s\} = \{0.9,0.1\}$. The target phase was $\Phi_0 = 0°$ (dashed), and the solutions in the final iteration (black) are tightly grouped along Φ_0. Figs. 7(b-c) indicate the mean (orange) in both phase and T begin to plateau around $N_{iter} = 17$, and at this point the phase evolution of a single population (blue) ceases to oscillate rapidly, settling around Φ_0.

The "best" design was chosen for its accuracy in Φ_0, and produced the unit cell seen in Fig.8(a), giving $\Phi = -0.15°$ and $T = 0.52$. Of note, the phase and transmission through the unadorned Si structure was $\Phi \approx -120°$ and $T \approx 0.75$ for this periodicity and wall thickness.

While there are no closed loops, there are fabrication concerns where two metal voxels are touching only at the corners, which is not physically conceivable. Depending on how the membrane mask is generated, these corners will "fuse" together or recede to the point where they no longer touch. This is a concern, as we see in

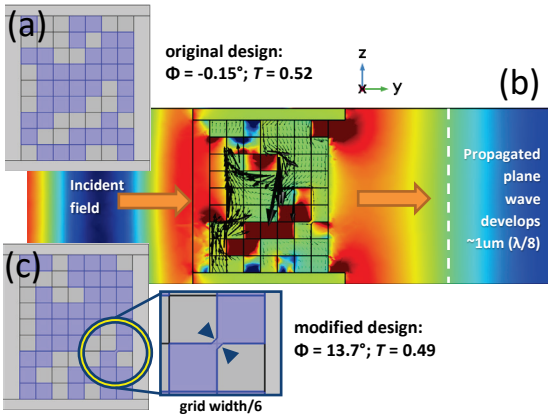

Figure 8. (a) Grid layout from "best" solution given in Fig.8(a); (b) $\boldsymbol{H_x}$ field and current; (c) modified design.

the H_x (color) and current density (arrow) in Fig.8(b) that this is where the current contributes the strongest. It has been found so far that small fused corners, as demonstrated in Fig.8(c) does not contribute severely to the results; in this case, a shift to $\Phi = 13.7°$ and $T = 0.49$ was observed. However, opening the gap cuts off current flow and skews the result greatly (not shown), and will be avoided in final designs.

6. Discussion

From a performance/design standpoint, the COMSOL-based GA routine delivered a solution that met technical goals in phase and amplitude, and demonstrated a robustness in how a multitude of architectures could be employed, whether isolated in free space or embedded in a complex half-space; symmetrical or asymmetrical; or single faced or multi-faced. Fabrication concerns may ultimately require alterations to any final design or hinder efficiencies. However, it is not difficult to introduce perturbations such as fusing

of corners into the COMSOL model to generate a more accurate result. Furthermore, the square voxels can evolve to shapes that do not permit corner contact, such as hexagons or octagons.

From a computational standpoint, the successful implementation of a GA routine into complex electromagnetic design introduces a great savings for the user, by precluding the need for lengthy parametric sweeps. This is an important point—the GA *automatically* picks the optimal design that works for the desired wavelength and geometrical boundaries *without* having to sweep the spectrum or a range of physical parameters! We did not include a quantitative study on time savings, as it becomes ultimately prohibitive to include all voxel combinations—but this statement alone infers the benefit. The GA routine also allows for scatterer geometries that conventional intuition typically cannot predict as optimal—which is a common GA benefit—now available for computational models through COMSOL, rather than limited to analytical models.

7. Conclusions

With COMSOL Multiphysics as the underlying computational mechanism, and bi-directional process link via LiveLink for MATLAB, a robust GA routine was successfully validated against a simple unit cell model, and then used to produce optimized solution spaces for design of a metasurface lens. Individual phase points were targeted accurately, and can be used to form the non-uniform phase profile required for lensing through a single, flat interface. Simulated transmissivities were >20% above the limitations imposed by linear polarization conversion. While fabrication feasibility is unproven, nevertheless COMSOL was instrumental in demonstrating that a GA routine can generate a single-layer 3-D plasmonic structure capable of significantly exceeding the physical limitations imposed by a 2-D planar architectures for improved metasurface optical applications.

8. References

[1] N. Yu and F. Capasso, "Flat optics with designer metasurfaces," *Nat Mater*, **13**, 139 (2014)

[2] M. Khorasaninejad *et al*., "Metalenses at Visible Wavelengths: Diffraction-Limited Focusing and Subwavelength Resolution Imaging," *Science,* **352**, 6290 (2016).

[3] A. Arbabi *et al*., "Subwavelength-Thick Lenses with High Numerical Apertures and Large Efficiency Based on High-Contrast Transmitarrays," *Nat Commun,* **6**, 7069 (2015).

[4] A. Arbabi and A. Faraon, "Fundamental Limits of Ultrathin Metasurface," *Sci Rep,* **7**, 43722 (2017).

[5] F. Monticone, *et al.*, "Full Control of Nanoscale Optical Transmission with a Composite Metascreen," *Phys Rev Lett,* **110**, 203903 (2013).

[6] N. Yu *et al*., "Light Propagation with Phase Discontinuities: Generalized Laws of Reflection and Refraction," *Science,* **334**, 333 (2011).

[7] N. Yu *et al*., "Flat Optics: Controlling Wavefronts with Optical Antenna Metasurfaces," IEEE J. Sel. Topics Quantum Electron., **19**, 3 (2013).

[8] F. Aieta, *et al.*, "Aberration-Free Ultrathin Flat Lenses and Axicons at Telecom Wavelengths Based on Plasmonic Metasurfaces," *Nano Lett*, **12**, 9 (2012).

[9] B. Adomanis, *et al.*, "Design of Infrared Metasurfaces for Low-Profile Optics Using COMSOL Multiphysics," COMSOL Conference Technical Papers (2016).

[10] C. Balanis, Antenna Theory: Analysis and Design, 4th ed., JWS (2016).

[11] R. Haupt and D. Werner, Genetic Algorithms for Electromagnetics, New York: JWS (2007).

[12] Y. Rahmat-Samii and E. Michielssen, Electromagnetic Optimization by Genetic Algorithms, New York: JWS (1999).

[13] D. B. Burckel *et al.,* "Micrometer-Scale Cubic Unit Cell 3D Metamaterial Layers," *Adv Mater*, 22, 5053 (2010).

9. Acknowledgements

We would like to acknowledge support from the Air Force Office of Scientific Research.